Structural Engineering and Mechanics, Vol. 45, No.3 (2013) 355-371
DOI: http://dx.doi.org/10.12989/sem.2013.45.3.355

Axisymmetrical bending of single- and multi-span functionally graded hollow cylinders

Z.G. Bian and Y.H. Wang*

Ningbo Institute of Technology, Zhejiang University, Ningbo 315100, P.R. China

(Received August 19, 2011, Revised November 26, 2012, Accepted December 16, 2012)

Abstract. Single- and multi-span orthotropic functionally graded hollow cylinders subjected to axisymmetrical bending are investigated on the basis of a unified shear deformable shell theory, in which the transverse displacement is expressed by means of a general shape function. To approach the through-thickness inhomogeneity of the hollow cylinder, a laminated model is employed. The shape function therefore shall be determined for each fictitious layer. To improve the computational efficiency, we resort to a transfer matrix method. Based on the principle of minimum potential energy, equilibrium equations are established, which are then solved analytically using the transfer matrix method for arbitrary boundary conditions. Numerical comparisons among a third-order shear deformable shell theory, an exact elastic theory and the present theory are provided for a simply supported hollow cylinder, from which the present theory turns out to be superior in stress estimation. Distributions of displacements and stresses in single- and three-span hollow cylinders with different boundary conditions are also illustrated in numerical examples.

Keywords: axisymmetrical bending; multi-span; hollow cylinder; functionally graded material; unified shear deformable shell theory; transfer matrix method

1. Introduction

The concept of functionally graded materials (FGMs) was first introduced by Niino *et al*. in 1984 (Koizumi 1997), and studies on FGMs were initiated from then on. Generally, FGMs possess spatially dependent mechanical properties resulting from their volume fractions changing with dimensions. They were firstly prepared for thermal barrier materials in aerospace to withstand thermal stresses (Kokini *et al*. 2002), but now the applications of FGMs are widely extended into many fields, including sensors and transducers (Müller *et al*. 2003), biomedical materials (Pompe *et al*. 2003, Watari *et al*. 2004), turbine rotors (Qian and Dutta 2003), welding materials (Miyamoto *et al*. 1999), nuclear reactors (Na and Kim 2009), etc.

Among the applications mentioned above, structural elements made of FGMs are frequently encountered, and many researchers had focused on the behaviors of FGM beams, plates, cylinders, panels and so on. For example, based on a higher-order shear theory, static analysis of a moderately thick FGM beam was implemented by Kadoli *et al*. (2008). Employing a displacement

*Corresponding author, Ph.D., E-mail: wangyh7244@nit.zju.edu.cn

function developed by themselves, Woodward and Kashtalyan (2011) obtained an exact three dimensional elasticity solution for bending of an FGM plate. Vel (2010) incorporated displacement method with power series method and presented an analytical elasticity solution for free vibrations of simply supported FGM cylindrical shells. Based on a first-order shear deformation theory, Aghdam *et al*. (2011) carried out a study on bending of moderately thick clamped FGM conical panels. In fact, some research works on this topic were also achieved by the authors (Bian *et al*. 2005, Bian *et al*. 2010, Bian *et al*. 2006a, Bian *et al*. 2006b, Chen *et al*. 2003, Chen *et al*. 2004).

In the present paper, we discuss an orthotropic functionally graded hollow cylinder (FGHC) subjected to axisymmetrical bending. Generally, classical shell theories were developed on the basis of the Kirchhoff-Love assumptions of straight inextensional normals. To accurately analyze the response of moderately thick shells, kinds of higher-order theories were suggested. Although these theories were applied to homogeneous shells in the beginning, they were also extended to analyze the inhomogeneous FGHC. For example, using Love's shell theory, Loy *et al*. (1999) studied the vibration characteristics of simply supported FGM cylindrical shells and influence of some material parameters on the natural frequencies were discussed. Pradhan *et al*. (2000) further investigated the vibration characteristics of FGM cylindrical shells with different boundary conditions. Both eigenvalue governing equations in the two papers were deduced by Rayleigh-Ritz method. Wu *et al*. (2005) analyzed the thermoelastic stability of FGM cylindrical shells by the Donnell's shell theory. For simply supported boundary conditions, closed form solutions for the critical buckling temperature differences of shells were achieved. Incorporating Sander's first-order shear deformation shell theory with the element-free *kp*-Ritz method, Zhao *et al*. (2009) analyzed the thermoelastic behavior and vibration of FGM cylindrical shells. A circular cylindrical shell composed of one middle FGM layer and two inner and outer homogeneous layers was studied by Li *et al*. (2010), where Flügge's shell theory was employed and natural frequency for simply supported boundary conditions was obtained. Bahtui and Eslami (2007) applied a second-order shear deformation shell theory to analyze the response of an FGM axisymmetric cylindrical shell in thermal environment. In space domain and in time domain, a Galerkin finite element method and the Laplace transform were used respectively. Matsunaga (2009) presented a 2D higher-order deformation theory to study the free vibration and stability of FGM circular cylindrical shells, where the governing equations were derived by virtue of Hamilton's principle and the power series expansion technique.

As we know, shear stresses in laminated structures are key parameters of analyzing multiple debondings and interfacial fractures (Andrews *et al*. 2009). In these cases, conventional shell theories mentioned above will present unsatisfactory stress estimation. Soldatos and Timarci (1993) suggested a unified shear deformable shell theory by introducing a general shape function that is a-posteriori specified. In our previous work (Bian *et al*. 2005), we found such shape function could alter with the through-thickness distribution of FGM components and satisfied stress results were obtained in numerical examples. In present paper, this shell theory is employed once more. For simply supported boundary conditions, numerical comparisons among the present shell theory, an exact elasticity theory and a third-order shear deformation shell theory are provided, and the superiority of the present theory in stress estimation is demonstrated. The effect of boundary conditions on the elastic fields in an FGHC is also illustrated in numerical examples. During the process, we apply a laminate model (Chen *et al*. 2003, 2004) to deal with the through-thickness inhomogeneity. That is, the FGHC is divided into N fictitious thin layers and each layer approximates to a homogeneous one. According to the shell theory of Soldatos and Timarci (1993), we now have to solve $2N$ simultaneous equations to determine the shape function.

Obviously, it will be very time-consuming if N increases. So we resort to a transfer matrix method (TMM, Bian *et al*. 2005), by virtue of which only two simultaneous equations are required when determining the shape function, regardless of how many fictitious layers are involved. To deal with the boundary conditions conveniently, governing equations are also solved within the framework of TMM.

In engineering practice, such as aeroplane surfaces, slabs and cladding panels in civil engineering, decks in bridges and ships, stresses and displacements of structures are often wished to be reduced while applied loads remain unchanged. To satisfy this requirement, one can place intermediate supports within the structures. Theoretically, multi-span structures can be treated as structures with internal line supports. Veletsos and Newmark (1956) first investigated the free vibration of a two-span rectangular plate. From then on, many researchers had focused on this topic employing various analytical and numerical methods (Abrate and Foster 1995, Cheung and Zhou 1999, 2000, 2001, Kong and Cheung 1995, Lee and Ng 1995, Li 2003, Liew *et al*. 1995, Xiang *et al*. 2002a, 2002b, Zhou 1994). Most of the open literatures, however, are concerned with the vibration characteristics of multi-span plates, and studies on static behaviors of these structures are relatively few (Bian *et al*. 2005). As compared with the multi-span plates, multi-span cylindrical shells attracted much less attention, although they are frequently encountered in oil transportation, chemical industry, pipeline, nuclear and marine engineering. Huang and Hsu (1993) utilized a receptance theory to determine the frequencies and mode shapes of a spinning cylindrical shell with interior multi-point or multi-line supports. But study on the static response of a multi-span FGHC is not found within the author's knowledge. So in the final part of this paper, we discuss the axisymmetrical bending of a multi-span FGHC with arbitrary boundary conditions at its two ends. Although the present method can be readily extended to analyze an FGHC with arbitrary spans, a three-span FGHC is chosen to demonstrate the through-span distributions of displacements and stresses.

2. Basic equations for a single-span FGHC

The functionally graded hollow cylinder investigated here is shown in Fig. 1, where cylindrical coordinates (r, θ, z) are established. Let L denote the length of the cylinder, and r_0, r_m and r_1 denote the inner, mean and outer radius, respectively. For an FGHC, the material properties are inhomogeneous along the radius, and the elastic parameters, c_{ij} s, can be expressed as

$$c_{ij} = c_{ij}(r) \tag{1}$$

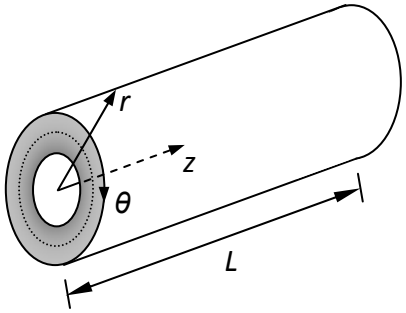

Fig. 1 Functionally graded hollow cylinder and its cylindrical coordinates

Suppose the FGHC is orthotropic, whose constitutive equations in cylindrical coordinates are

$$\begin{Bmatrix} \sigma_{zz} \\ \sigma_{\theta\theta} \\ \sigma_{rr} \\ \sigma_{r\theta} \\ \sigma_{zr} \\ \sigma_{\theta z} \end{Bmatrix} = \begin{bmatrix} c_{11} & c_{12} & c_{13} & 0 & 0 & 0 \\ c_{12} & c_{22} & c_{23} & 0 & 0 & 0 \\ c_{13} & c_{23} & c_{33} & 0 & 0 & 0 \\ 0 & 0 & 0 & c_{44} & 0 & 0 \\ 0 & 0 & 0 & 0 & c_{55} & 0 \\ 0 & 0 & 0 & 0 & 0 & c_{66} \end{bmatrix} \begin{Bmatrix} \varepsilon_{zz} \\ \varepsilon_{\theta\theta} \\ \varepsilon_{rr} \\ \varepsilon_{r\theta} \\ \varepsilon_{zr} \\ \varepsilon_{\theta z} \end{Bmatrix} \tag{2}$$

where σ_{ij} and ε_{ij} ($i, j = r, \theta, z$) are components of the stresses and strains, respectively.

Consider the FGHC is in a state of axisymmetrical bending, the displacement in θ- dimension is then vanished, and all mechanical quantities are independent of θ. According to the shell theory suggested by Soldatos and Timarci (1993), the non-zeroes displacements are assumed to be

$$\begin{aligned} U_z &= u_z - (r - r_m)\frac{du_r}{dz} + \varphi_z \cdot \gamma_z \\ U_r &= u_r \end{aligned} \tag{3}$$

where U_z and U_r are displacements in z- and r-directions, respectively. u_z, u_r and γ_z are displacements and transverse shear strain at middle shell ($r = r_m$), respectively. Unlike most conventional shell theories, the shape function, φ_z, in Eq. (3) is a-posteriori specified.

By virtue of the principle of minimum potential energy, one can establish the following equilibrium equations

$$\frac{dN_z}{dz} = 0, \quad q_\theta - \frac{d^2 M_z}{dz^2} = r_1 q_1 + r_0 q_0, \quad \frac{dM_z^a}{dz} - Q_z^a = 0 \tag{4}$$

where q_0 and q_1 are normal loads applying on the inner and outer surfaces, respectively, and the generalized resultant forces are denoted as

$$\begin{aligned} &N_z = \int_{r_0}^{r_1} \sigma_{zz} r dr, \quad q_\theta = \int_{r_0}^{r_1} \sigma_{\theta\theta} dr, \quad M_z = \int_{r_0}^{r_1} \sigma_{zz}(r - r_{\mathrm{m}}) r dr, \quad M_z^a = \int_{r_0}^{r_1} \varphi_z \sigma_{zz} r dr \\ &Q_z^a = \int_{r_0}^{r_1} (d\varphi_z / dr) \sigma_{zr} r dr \end{aligned} \tag{5}$$

Meanwhile, the boundary conditions at $z = 0$ and $z = L$ are derived

$$\begin{aligned} &N_z = 0 \ \text{ or } \ u_z \ \text{ is prescribed}; \quad Q_z = 0 \ \text{ or } \ u_r \ \text{ is prescribed} \\ &M_z^a = 0 \ \text{ or } \ \gamma_z \ \text{ is prescribed}; \quad M_z = 0 \ \text{ or } \ \alpha \ \text{ is prescribed} \end{aligned} \tag{6}$$

where $Q_z = dM_z / dz$ and $\alpha = du_r / dz$. In present study, the following typical boundary conditions are discussed

$$\begin{aligned}&\text{Clamped (C):}\ \ u_z=0,\ \ u_r=0,\ \ \gamma_z=0,\ \ \alpha=0\\&\text{Free (F):}\ \ N_z=0,\ \ Q_z=0,\ \ M_z^a=0,\ \ M_z=0\\&\text{Simply supported (S):}\ \ N_z=0,\ \ u_r=0,\ \ M_z^a=0,\ \ M_z=0\end{aligned}\tag{7}$$

The equilibrium equations with different boundary conditions can be solved by the TMM conveniently. To do so, we expand the resultant forces in Eq. (5) as

$$\begin{aligned}&N_z=C_{11}\frac{du_z}{dz}-C_{13}\frac{d\alpha}{dz}+C_{14}\frac{d\gamma_z}{dz}+C_{21}u_r,\ \ q_\theta=C_{21}\frac{du_z}{dz}-C_{23}\frac{d\alpha}{dz}+C_{22}\frac{d\gamma_z}{dz}+C_{31}u_r\\&M_z=C_{13}\frac{du_z}{dz}-C_{16}\frac{d\alpha}{dz}+C_{15}\frac{d\gamma_z}{dz}+C_{23}u_r,\ \ M_z^a=C_{14}\frac{du_z}{dz}-C_{15}\frac{d\alpha}{dz}+C_{12}\frac{d\gamma_z}{dz}+C_{22}u_r\\&Q_z^a=C_{51}\gamma_z\end{aligned}\tag{8}$$

where the coefficients are defined as

$$\begin{aligned}&C_{11}=\int_{r_0}^{r_1}c_1rdr,\ \ C_{12}=\int_{r_0}^{r_1}c_1\varphi_z^2rdr,\ \ C_{13}=\int_{r_0}^{r_1}c_1(r-r_m)rdr,\ \ C_{14}=\int_{r_0}^{r_1}c_1\varphi_zrdr\\&C_{15}=\int_{r_0}^{r_1}c_1\varphi_z(r-r_m)rdr,\ \ C_{16}=\int_{r_0}^{r_1}c_1(r-r_m)^2rdr,\ \ C_{21}=\int_{r_0}^{r_1}c_2dr,\ \ C_{22}=\int_{r_0}^{r_1}c_2\varphi_zdr\\&C_{23}=\int_{r_0}^{r_1}c_2(r-r_m)dr,\ \ C_{31}=\int_{r_0}^{r_1}\frac{c_3}{r}dr,\ \ C_{51}=\int_{r_0}^{r_1}\frac{\phi_z^2}{c_5}rdr\end{aligned}\tag{9}$$

in which $c_1=c_{11}-c_{13}^2/c_{33}$, $c_2=c_{12}-c_{13}c_{23}/c_{33}$, $c_3=c_{22}-c_{23}^2/c_{33}$, $c_5=c_{55}$ and $\phi_z=c_5d\varphi_z/dr$. Obviously, all coefficients can be calculated by numerical integrations.

Once a sate vector composed of the quantities appearing in the boundary conditions is chosen, we can formulate a set of state equations from Eqs. (4) and (8)

$$\mathbf{D}\frac{d\mathbf{V}}{dz}=\mathbf{Z}\cdot\mathbf{V}+\mathbf{S}\tag{10}$$

where

$$\mathbf{V}=[u_z,u_r,\gamma_z,\alpha,N_z,Q_z,M_z^a,M_z]^T,\ \ \mathbf{S}=[0,0,0,0,0,0,r_1q_1+r_0q_0,0]^T$$

$$\mathbf{D}=\begin{bmatrix}0&1&0&0&0&0&0&0\\0&0&0&0&0&0&0&1\\C_{11}&0&C_{14}&-C_{13}&0&0&0&0\\C_{13}&0&C_{15}&-C_{16}&0&0&0&0\\C_{14}&0&C_{12}&-C_{15}&0&0&0&0\\0&0&0&0&1&0&0&0\\C_{21}&0&C_{22}&-C_{23}&0&-1&0&0\\0&0&0&0&0&0&1&0\end{bmatrix},\ \ \mathbf{Z}=\begin{bmatrix}0&0&0&1&0&0&0&0\\0&0&0&0&0&1&0&0\\0&-C_{21}&0&0&1&0&0&0\\0&-C_{23}&0&0&0&0&0&1\\0&-C_{22}&0&0&0&0&1&0\\0&0&0&0&0&0&0&0\\0&-C_{31}&0&0&0&0&0&0\\0&0&C_{51}&0&0&0&0&0\end{bmatrix}\tag{11}$$

Eq. (10) can be solved readily as follows

$$\mathbf{V}(z)=\exp(z\mathbf{D}^{-1}\mathbf{Z})\cdot\mathbf{V}(0)+\int_0^z\exp[(z-\tau)\mathbf{D}^{-1}\mathbf{Z}]\cdot\mathbf{D}^{-1}\mathbf{S}(\tau)d\tau \tag{12}$$

From Eq. (12), the following relationship between the state vectors at two ends of FGHC is derived

$$\mathbf{V}(L)=\boldsymbol{\chi}\cdot\mathbf{V}(0)+\boldsymbol{\lambda} \tag{13}$$

in which

$$\boldsymbol{\chi}=\exp(L\mathbf{D}^{-1}\mathbf{Z}),\qquad \boldsymbol{\lambda}=\int_0^L\exp[(L-\tau)\mathbf{D}^{-1}\mathbf{Z}]\cdot\mathbf{D}^{-1}\mathbf{S}(\tau)d\tau \tag{14}$$

According to Eq. (7), four elements of V(0) and four elements of V(L) are prescribed, making use of which, the other four elements of V(0) can be determined. Finally any V(z) can be solved from Eq. (12).

3. Basic equations for a multi-span FGHC

An FGHC with n-span is shown in Fig. 2, where $\mathbf{V}_i^-$ and $\mathbf{V}_i^+$ denote the state vectors at left and right ends of the ith-span, respectively. As known from Eq. (13), they satisfy

$$\mathbf{V}_i^+=\boldsymbol{\chi}_i\cdot\mathbf{V}_i^-+\boldsymbol{\lambda}_i,\qquad i=1,2,\cdots,n \tag{15}$$

At each internal support, the shear force, Q_z, is discontinuous and the deflection, u_r, is vanished, which bring out the following equations

$$\boldsymbol{\kappa}_1\cdot\mathbf{V}_i^+=\boldsymbol{\kappa}_2\cdot\mathbf{V}_{i+1}^- \tag{16}$$

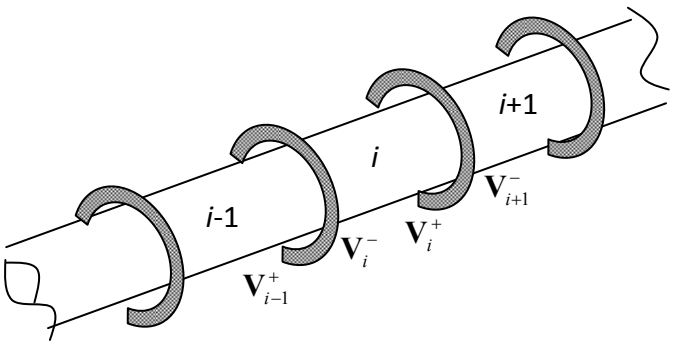

Fig. 2 Schematic model of a multi-span functionally graded hollow cylinder

where

$$\boldsymbol{\kappa}_1 = \begin{bmatrix} 1 & 0 & 0 & 0 & 0 & 0 & 0 & 0 \\ 0 & 1 & 0 & 0 & 0 & 0 & 0 & 0 \\ 0 & 0 & 1 & 0 & 0 & 0 & 0 & 0 \\ 0 & 0 & 0 & 1 & 0 & 0 & 0 & 0 \\ 0 & 0 & 0 & 0 & 1 & 0 & 0 & 0 \\ 0 & 1 & 0 & 0 & 0 & 0 & 0 & 0 \\ 0 & 0 & 0 & 0 & 0 & 0 & 1 & 0 \\ 0 & 0 & 0 & 0 & 0 & 0 & 0 & 1 \end{bmatrix}, \quad \boldsymbol{\kappa}_2 = \begin{bmatrix} 1 & 0 & 0 & 0 & 0 & 0 & 0 & 0 \\ 0 & 1 & 0 & 0 & 0 & 0 & 0 & 0 \\ 0 & 0 & 1 & 0 & 0 & 0 & 0 & 0 \\ 0 & 0 & 0 & 1 & 0 & 0 & 0 & 0 \\ 0 & 0 & 0 & 0 & 1 & 0 & 0 & 0 \\ 0 & 0 & 0 & 0 & 0 & 0 & 0 & 0 \\ 0 & 0 & 0 & 0 & 0 & 0 & 1 & 0 \\ 0 & 0 & 0 & 0 & 0 & 0 & 0 & 1 \end{bmatrix} \tag{17}$$

Combining Eqs. (15) and (16) for all spans, we obtain a set of equations

$$\begin{bmatrix} \boldsymbol{\chi}_1 & -\mathbf{I} & & & & \\ & \boldsymbol{\kappa}_1 & -\boldsymbol{\kappa}_2 & & & \\ & & \cdots & & & \\ & & & \boldsymbol{\kappa}_1 & -\boldsymbol{\kappa}_2 & \\ & & & & \boldsymbol{\chi}_n & -\mathbf{I} \end{bmatrix}_{(16n-8)\times(16n)} \begin{Bmatrix} \mathbf{V}_1^- \\ \mathbf{V}_1^+ \\ \mathbf{V}_2^- \\ \vdots \\ \mathbf{V}_{n-1}^+ \\ \mathbf{V}_n^- \\ \mathbf{V}_n^+ \end{Bmatrix}_{(16n)\times 1} = \begin{Bmatrix} -\boldsymbol{\lambda}_1 \\ \mathbf{0} \\ -\boldsymbol{\lambda}_2 \\ \vdots \\ -\boldsymbol{\lambda}_{n-1} \\ \mathbf{0} \\ -\boldsymbol{\lambda}_n \end{Bmatrix}_{(16n-8)\times 1} \tag{18}$$

where I and 0 are eighth-order identity matrix and eighth-order null vector, respectively.

To take into account the boundary conditions at two ends of this multi-span FGHC, we insert the equations described in Eq. (7) into Eq. (18), the state vectors, $\mathbf{V}_1^-, \mathbf{V}_1^+, \cdots, \mathbf{V}_n^+$, can be therefore solved, and the state vectors at any positions can be determined by virtue of Eq. (12).

4. Determination of the shape function

Obviously, the accuracy of the present theory will depend deeply on the form of the shape function. The physical meaning of φ_z leads to the following equations (Soldatos and Watson 1997)

$$\varphi_z = 0, \quad \frac{d\varphi_z}{dr} = 1, \text{ at } \; r = r_m \tag{19}$$

When normal loads apply on the inner and outer surfaces of a hollow cylinder, shear stresses at these two surfaces will be vanished, so φ_z also satisfies with

$$\frac{d\varphi_z}{dr} = 0 \quad \text{at} \quad r = r_0 \quad \text{and} \quad r = r_1 \tag{20}$$

To determine the distribution of φ_z, we employ the following three-dimensional equation of equilibrium

$$\frac{\partial \sigma_{zz}}{\partial z}+\frac{\partial \sigma_{zr}}{\partial r}+\frac{\sigma_{zr}}{r}=0 \tag{21}$$

It is troublesome to solve Eq. (21) directly, since the FGHC is inhomogeneous through thickness. So we resort to a laminate model here, on the basis of which, an FGHC is divided equally into 2*N* fictitious piece layers, and each layer approximates to a homogeneous one. In what follows, the elastic constants of each layer take their values at the mid-position of that layer.

By virtue of the constitutive equations and geometrical equations, Eq. (21) is transformed into the following equation within a layer

$$c_1\frac{d^2u_z}{dz^2}-c_1(r-r_m)\frac{d^3u_r}{dz^3}+\frac{c_2}{r}\frac{du_r}{dz}+c_1\varphi_z\frac{d^2\gamma_z}{dz^2}+\gamma_z\left(\frac{d\phi_z}{dr}+\frac{\phi_z}{r}\right)=0 \tag{22}$$

Clearly, the coefficients in Eq. (22) are different for all 2*N* layers, which makes it very time-consuming to determine the shape function. So we adopt TTM again to improve computational efficiency.

A particular solution to Eq. (22) is chosen as

$$u_z=A\cos(m\pi z/L),\ \ u_r=B\sin(m\pi z/L),\ \ \gamma_z=\cos(m\pi z/L) \tag{23}$$

Substituting Eq. (23) into Eq. (22) and rearranging the variables, we can get the following space equations

$$\frac{d}{dr}\begin{Bmatrix}\varphi_z\\ \phi_z\end{Bmatrix}=\mathbf{T}_i\begin{Bmatrix}\varphi_z\\ \phi_z\end{Bmatrix}+\mathbf{P}_iA-\mathbf{Q}_iB \tag{24}$$

with the coefficient matrixes

$$\mathbf{T}_i=\begin{bmatrix}0 & 1/c_5\\ c_1\beta^2 & -1/r\end{bmatrix}_i,\ \ \mathbf{P}_i=\begin{Bmatrix}0\\ c_1\beta^2\end{Bmatrix}_i,\ \ \mathbf{Q}_i=\begin{Bmatrix}0\\ c_1(r-r_{\mathrm{m}})\beta^3+\dfrac{c_2}{r}\beta\end{Bmatrix}_i,\ \ i=1,2,\cdots,2N \tag{25}$$

where $\beta=m\pi/L$, and the subscript *i* indicates the coefficient matrix takes its value in the *i*th layer.

The solution to Eq. (24) is

$$\begin{Bmatrix}\varphi_z\\ \phi_z\end{Bmatrix}=\exp[\mathbf{T}_i(r-r_i^-)]\cdot\begin{Bmatrix}\varphi_z\\ \phi_z\end{Bmatrix}_i^-+A\left\{\int_{r_i^-}^{r}\exp[\mathbf{T}_i(r-\tau)]\mathbf{P}_i d\tau\right\}-B\left\{\int_{r_i^-}^{r}\exp[\mathbf{T}_i(r-\tau)]\mathbf{Q}_i d\tau\right\}$$
$$r_i^-\le r\le r_i^+ \tag{26}$$

where $r_i^-=(i-1)(r_1-r_0)/(2N)+r_0$, $r_i^+=i(r_1-r_0)/(2N)+r_0$ and $\begin{Bmatrix}\varphi_z\\ \phi_z\end{Bmatrix}_i^-$ represents a state vector at $r=r_i^-$. Due to the continuity of displacement, U_z, and shear stress, σ_{zr}, at each fictitious interface, φ_z and φ_z are also continuous at that position, their relationship between any two

interfaces can be therefore obtained by a recursive method. Taking Eqs. (19) and (20) into account, we have

$$\begin{Bmatrix} 0 \\ (c_5)_N \end{Bmatrix} = \mathbf{H}_{N,1} \begin{Bmatrix} (\varphi_z)_1^- \\ 0 \end{Bmatrix} + A\mathbf{J}_{N,1} - B\mathbf{K}_{N,1}$$

$$\begin{Bmatrix} (\varphi_z)_{2N}^+ \\ 0 \end{Bmatrix} = \mathbf{H}_{2N,N+1} \begin{Bmatrix} 0 \\ (c_5)_N \end{Bmatrix} + A\mathbf{J}_{2N,N+1} - B\mathbf{K}_{2N,N+1} \tag{27}$$

where

$$\mathbf{H}_{i,j} = \exp(\frac{\mathbf{T}_i}{2N}), \quad \mathbf{J}_{i,j} = \mathbf{E}_i, \quad \mathbf{K}_{i,j} = \mathbf{F}_i \quad \text{for} \quad i = j$$

$$\mathbf{H}_{i,j} = \mathbf{H}_{i,j+1} \exp(\frac{\mathbf{T}_j}{2N}), \quad \mathbf{J}_{i,j} = \mathbf{H}_{i,j+1}\mathbf{E}_j + \mathbf{J}_{i,j+1}, \quad \mathbf{K}_{i,j} = \mathbf{H}_{i,j+1}\mathbf{F}_j + \mathbf{K}_{i,j+1} \quad \text{for} \quad i > j \tag{28}$$

in which

$$\mathbf{E}_i = \int_{r_i^-}^{r_i^+} \exp[\mathbf{T}_i(r_i^+ - \tau)]\mathbf{P}_i d\tau, \quad \mathbf{F}_i = \int_{r_i^-}^{r_i^+} \exp[\mathbf{T}_i(r_i^+ - \tau)]\mathbf{Q}_i d\tau \tag{29}$$

From Eq. (27), $(\varphi_z)_1^-$, A and B are solved, the shape function at any position can be therefore determined from Eq. (26).

5. Numerical examples

In what follows, we suppose each FGHC has the same geometric sizes as $r_0 / H = 20$ and $L / H = 3$, where $H = r_1 - r_0$. The outermost surface is free and the innermost surface is subjected to a sinusoidal load, namely $q_1 = 0$ and $q_0 = c_{44}^1 \sin(\pi H\zeta / L)$, in which $\zeta = z / H$ and c_{44}^1 represents the value of c_{44} on the outermost surface.

Before the numerical calculation, the distribution model of an FGHC must be defined. Herein we assume

$$\Psi = \Psi_1(\Psi_0 / \Psi_1)^\mu \tag{30}$$

where $\mu = (\eta_1 - \eta)^p$, $\eta = r / H$ and p is a gradient index. Ψ denotes one of the elastic constants, Ψ_0 and Ψ_1 are the corresponding ones for two homogeneous materials, which are listed in Table 1. Fig. 3 illustrates the effect of gradient index on distributions of the elastic constant, c_{11}, from which we can see c_{11} keeps constant and the FGHC degenerates to a homogeneous one for $p = 0$, while for other values of p, c_{11} varies with the radius and the FGHC becomes inhomogeneous.

In Fig. 4, through-thickness distributions of shape functions with different gradient indexes are plotted, which demonstrates that the shape function in present theory will alter with not only the special coordinate but also the gradient index. As is known to all, the transverse shear

Table 1 Elastic constants of two homogenous materials (Units: 10^{10}N/m^2)

Elastic constant	c_{11}	c_{12}	c_{13}	c_{22}	c_{23}	c_{33}	c_{44}	c_{55}	c_{66}
Ψ_0	40.17	0.33	0.34	1.07	0.27	1.07	0.50	0.70	0.50
Ψ_1	15.98	0.47	0.47	1.20	1.20	1.20	0.55	0.42	0.42

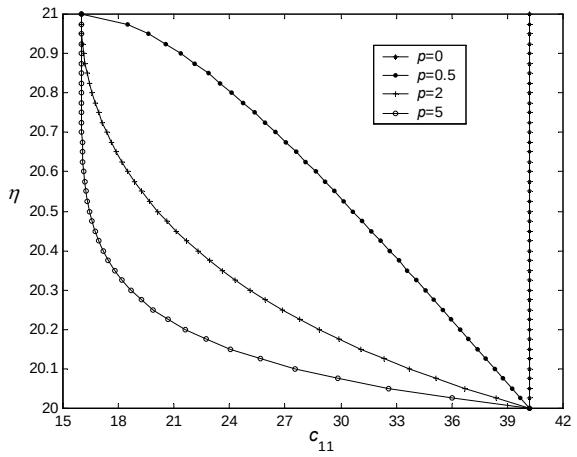

Fig. 3 Through-thickness distributions of c_{11} for different gradient indexes

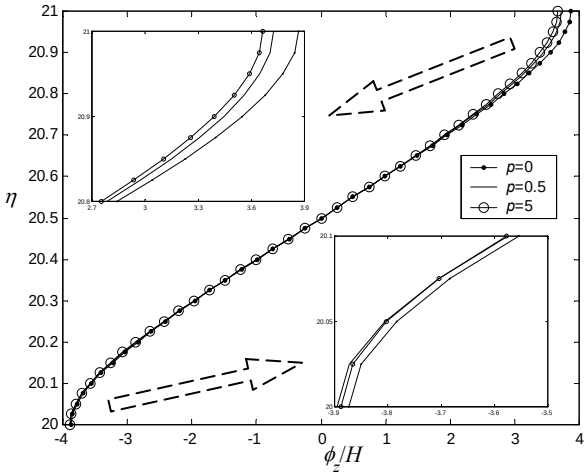

Fig. 4 Through-thickness distributions of shape functions for different gradient indexes

deformations of most conventional shell theories remain invariant once the assumptions of displacement fields are chosen, regardless of the variation of gradient index. Such self-adjustable characteristic of present theory is very suitable to analyze an inhomogeneous FGHC.

The present theory can unify most of shear deformable shell theories (Soldatos and Timarci 1993). For example, we can specify a particular shape function as

$$\varphi_z = (r - r_m)[1 - \frac{4}{3}(\frac{r - r_m}{r_1 - r_0})^2] \tag{31}$$

Obviously, Eq. (31) satisfies Eqs. (19) and (20). Such form of shape function corresponds with a third-order shear deformable shell theory.

Figs. 5 and 6 display the numerical comparisons among an exact elastic theory, the third-order shell theory and the present theory, where the single-span FGHC is simply supported at two edges and the gradient index p = 2. The exact elastic theory is directly based on three-dimensional equations of equilibrium and the governing equations are solved by a state space method, the details on this theory can be found in Chen *et al*. (2004). As compared with the third-order shell theory, the present theory possesses higher accuracy in predicting both normal and shear stresses. From Fig. 6, we also find even the third-order theory can not point out where the peak shear stress is. So the present theory owns more superiority in analyzing the mechanical behaviors of inhomogeneous or laminated structures.

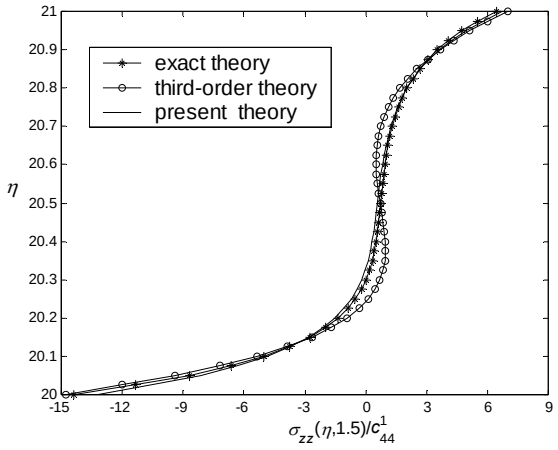

Fig. 5 Through-thickness distributions of normal stresses predicted by different theories

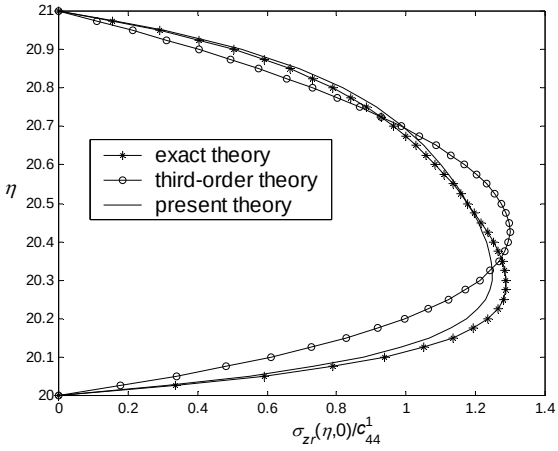

Fig. 6 Through-thickness distributions of shear stresses predicted by different theories

Now we investigate the axisymmetrical bending of a single-span FGHC. Figs. 7-10 present the spatial distributions of stresses with all reasonable combinations of boundary conditions at two ends, including both simply supported (SS), both clamped (CC), clamped-simply supported (CS) and clamped-free (CF). In these figures, the gradient index, p, is chosen as 0.5. As is expected, the boundary conditions have pronounced effect on the spatial distributions of stresses. In terms of peak normal stress (PNS) and peak shear stress (PSS), both the maximum of all PNSs and the maximum of all PSSs appear in an FGHC with CF boundary conditions, while the minimum of all PNSs and the minimum of all PSSs appear in an FGHC with SS and CC boundary conditions, respectively. As shown in these figures, bending stresses in the FGHC vary smoothly through thickness, which benefits from the continuous components of FGM and will therefore delay the failures resulted from stress concentration or interfacial debonding.

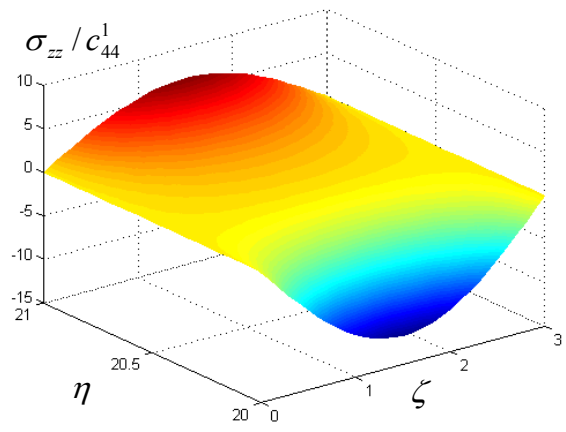

(a)

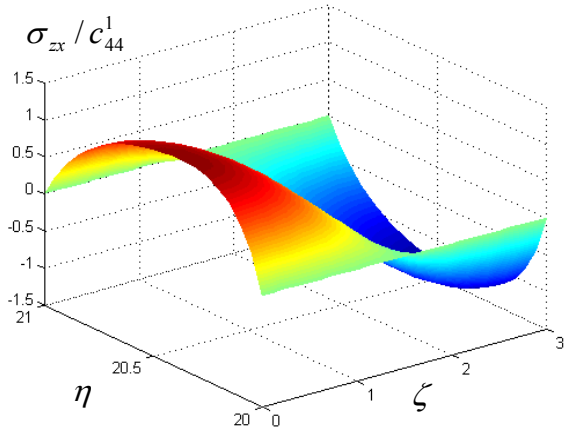

(b)

Fig. 7 Spatial distributions of stresses with SS boundary conditions (a) distribution of normal stress, (b) distribution of shear stress

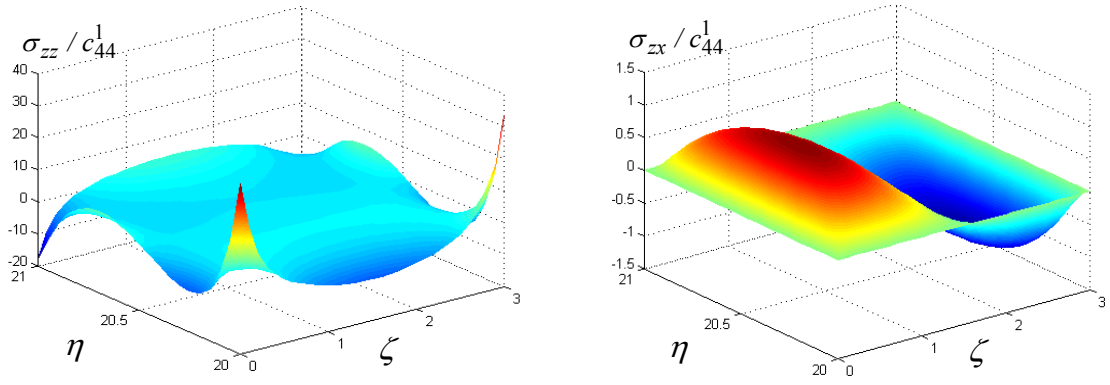

(a) (b)

Fig. 8 Spatial distributions of stresses with CC boundary conditions (a) distribution of normal stress, (b) distribution of shear stress

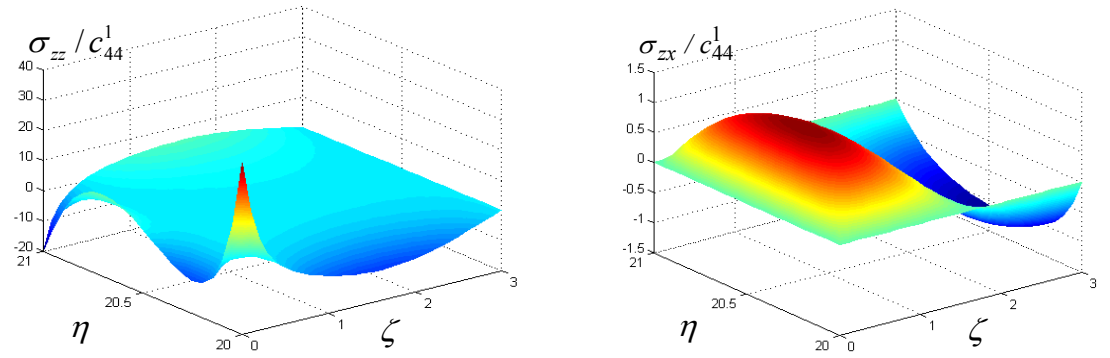

(a) (b)

Fig. 9 Spatial distributions of stresses with CS boundary conditions (a) distribution of normal stress, (b) distribution of shear stress

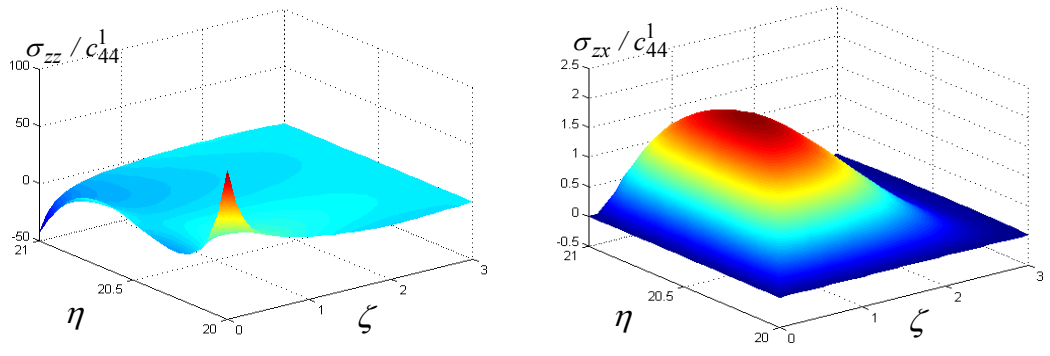

(a) (b)

Fig. 10 Spatial distributions of stresses with CF boundary conditions (a) distribution of normal stress, (b) distribution of shear stress

At the end, static responses of a three-span FGHC are calculated, where the gradient index p = 1. For brevity, each span has the same length-to-thickness ratio, namely $L / H = 3$, and is subjected to a same loading, namely $q_1 = 0$ and $q_0 = c_{44}^1 \sin(\pi H\zeta / L)$. Results of present FGHC with SS and CF boundary conditions are displayed in Figs. 11 and 12, respectively.

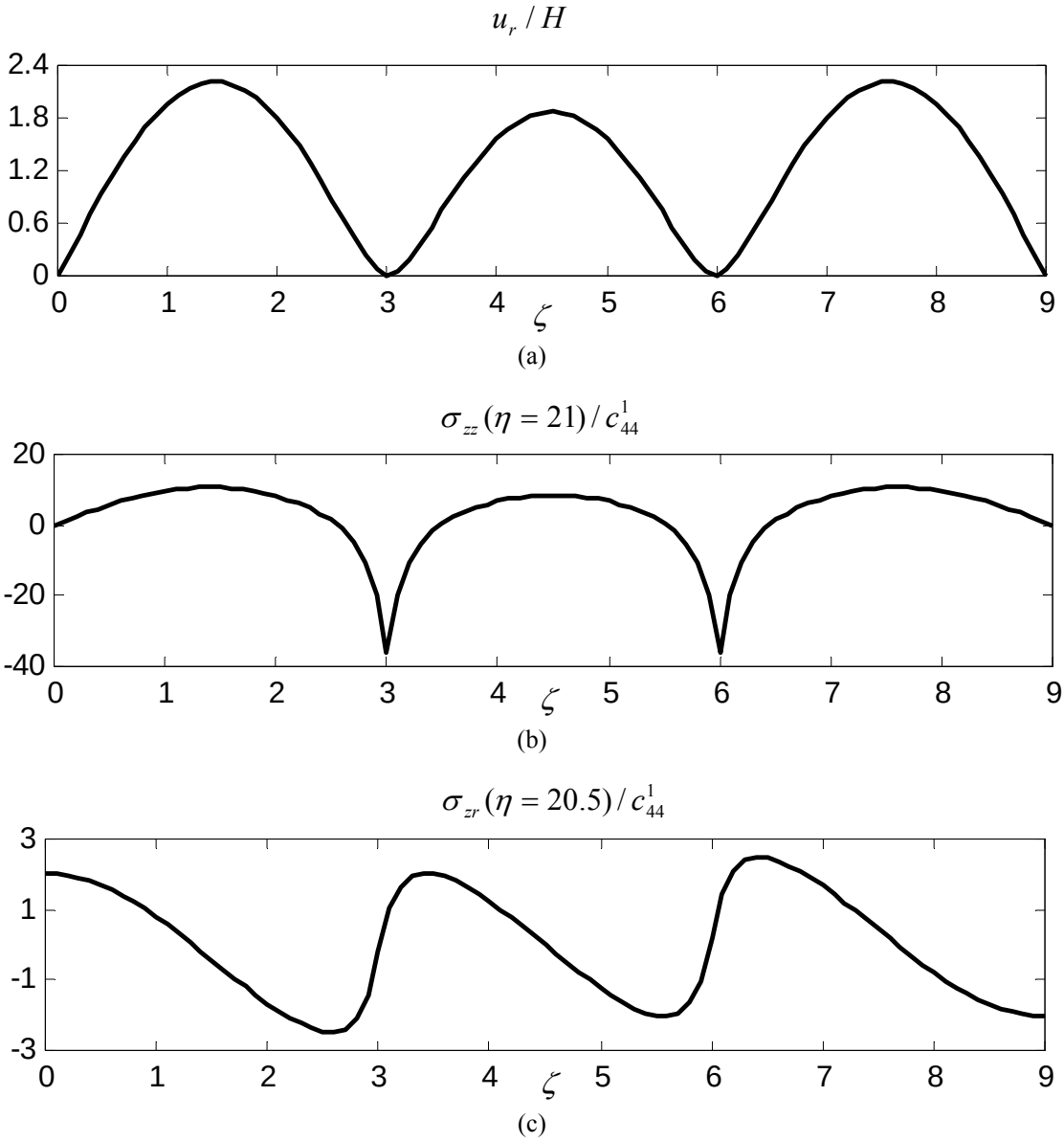

Fig. 11 Static responses of a three-span FGHC with SS boundary conditions (a) through-span distribution of deflection, (b) through-span distribution of normal stress, (c) through-span distribution of shear stress

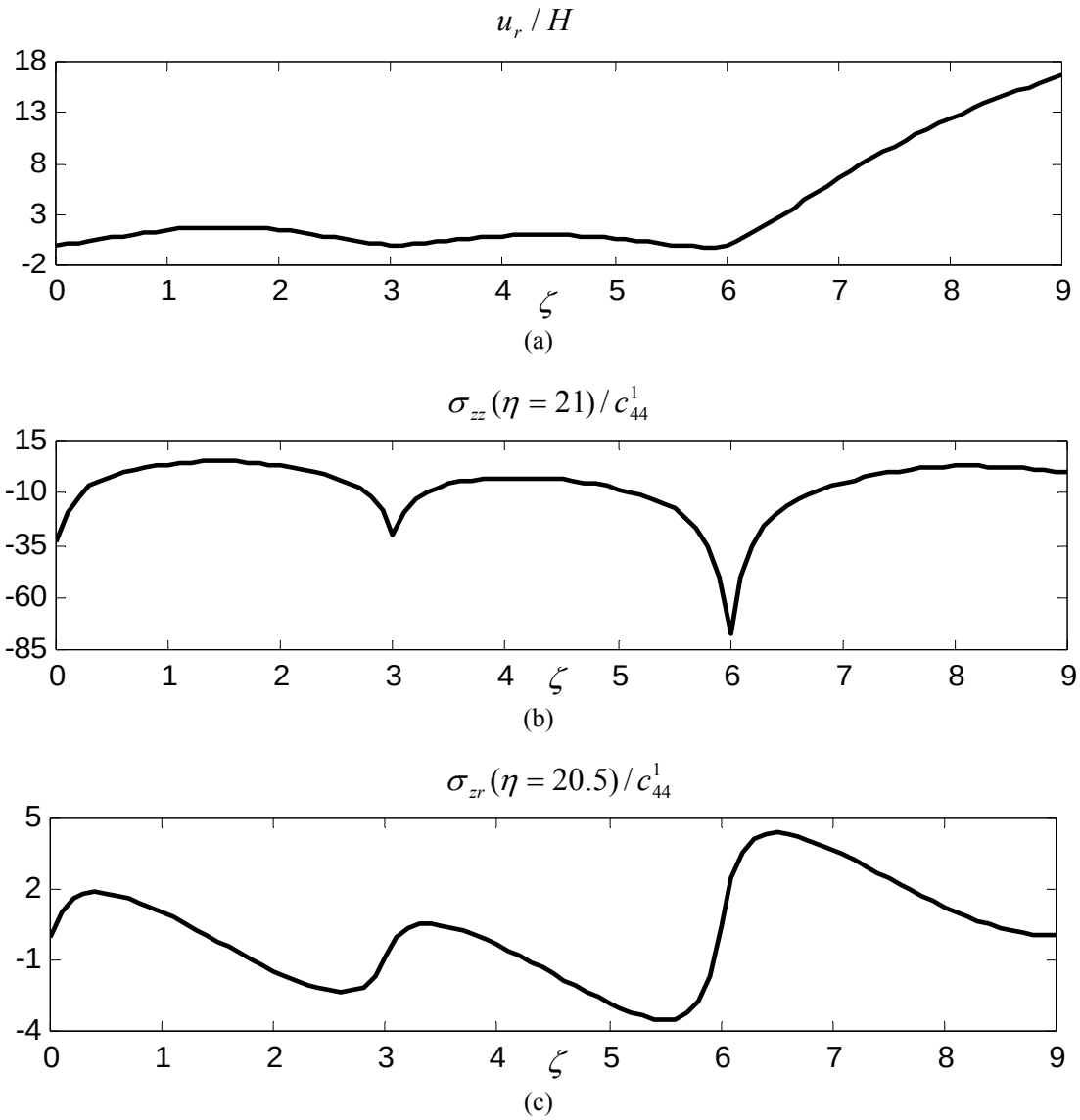

Fig. 12 Static responses of a three-span FGHC with CF boundary conditions (a) through-span distribution of deflection, (b) through-span distribution of normal stress, (c) through-span distribution of shear stress

6. Conclusions

In present paper, we extend a unified shear deformable shell theory suggested by Soldatos and Timarci (1993) to study the axisymmetrical bending of single- and multi-span FGHCs. Based on the principle of minimum potential energy, governing equations are obtained and solved by TMM. Due to the state vector adopted in TMM consists of all (generalized) resultants and (generalized) displacements encountered in boundary conditions, dealing with an FGHC with all reasonable combinations of boundary conditions becomes very convenient. For a multi-span FGHC, the state

vectors are discontinuous at internal supports, so we introduce two singular matrixes accounting for $u_r = 0$ as well as connecting two adjacent state vectors.

By virtue of a laminated model, the inhomogeneous FGHC is divided into many thin layers through thickness, and each layer approximates a homogeneous one. As a result, the shape function in present theory must be determined for each layer. To improve the computational efficiency, we employ the TMM again, owing to which, only two simultaneous equations are required to determine the shape function, regardless of how many fictitious layers are involved. Since the shape function is derived from a three-dimensional equation of equilibrium and is a-posteriori specified, it can alter with the inhomogeneous distributions of material properties, as is shown in the numerical example.

Numerical comparisons among an exact elastic theory, a third-order shear deformable shell theory and the present theory are achieved in this paper, and the superiority of present theory in predicting bending stresses is illustrated. For a single-span FGHC, the spatial distributions of stresses with four boundary conditions, namely SS, CC, CS and CF, are displayed. From these figures, we can see the bending stresses of FGHC vary smoothly through thickness due to the continuous components of FGM, which is beneficial to release interfacial stress concentration and therefore delay interfacial debonding. As is expected, the boundary conditions also have pronounced effect on the spatial distributions of stresses. Static responses of a three-span FGHC are calculated finally. For the sake of brevity, only two kinds of boundary conditions, i.e. SS and CF, are taken into account, although the present method can deal with other boundary conditions including SF, FF, CS and CC without any difficulties.

Acknowledgements

The work was supported by the Zhejiang Provincial Natural Science Foundation of China (no. Y6100234) and the National Natural Science Foundation of China (no. 50808160).

References

Abrate, S. and Foster, E. (1995), "Vibrations of composite plates with intermediate line supports", *J. Sound. Vib.*, 179, 793-815.

Andrews, M.G., Massabò, R., Cavicchi, A. and Cox, B.N. (2009), "Dynamic interaction effects of multiple delaminations in plates subject to cylindrical bending", *Int. J. Solid. Struct.*, **46**, 1815-1833.

Aghdam, M.M., Shahmansouri, N. and Bigdeli, K. (2011), "Bending analysis of moderately thick functionally graded conical panels", *Compos. Struct.*, **93**, 1376-1384.

Bahtui, A. and Eslami, M.R. (2007), "Coupled thermoelasticity of functionally graded cylindrical shells", *Mech. Res. Comm.*, **34**, 1-18.

Bian, Z.G., Chen, W.Q., Lim, C.W. and Zhang, N. (2005), "Analytical solutions for single- and multi-span functionally graded plates in cylindrical bending", *Int. J. Solid. Struct.*, **42**, 6433-6456.

Bian, Z.G., Chen, W.Q. and Zhao, J. (2010), "Steady-state response and free vibration of an embedded imperfect smart functionally graded hollow cylinder filled with compressible fluid", *Struct. Eng. Mech.*, **34**, 449-474.

Bian, Z.G., Lim, C.W. and Chen, W.Q. (2006a), "On functionally graded beams with integrated surface piezoelectric layers", *Compos. Struct.*, **72**, 339-351.

Bian, Z.G., Ying, J., Chen, W.Q. and Ding, H.J. (2006b), "Bending and free vibration analysis of a smart

functionally graded plate", *Struct. Eng. Mech.*, **23**, 97-113.
Chen, W.Q., Bian, Z.G. and Ding, H.J. (2003), "Three-dimensional analysis of a thick FGM rectangular plate in thermal environment", *Journal of Zhejiang University SCIENCE A*, **4**, 1-7.
Chen, W.Q., Bian, Z.G. and Ding, H.J. (2004), "Three-dimensional vibration analysis of fluid-filled orthotropic FGM cylindrical shells", *Int. J. Mech. Sci.*, **4**6, 159-171.
Cheung, Y.K. and Zhou, D. (1999), "Eigenfrequencies of tapered rectangular plates with intermediate line supports", *Int. J. Solid. Struct.*, **36**, 143-166.
Cheung, Y.K. and Zhou, D. (2000), "Vibrations of rectangular plates with elastic intermediate line-supports and edge constraints", *Thin-Walled Structures*, **37**, 305-331.
Cheung, Y.K. and Zhou, D. (2001), "Vibration analysis of symmetrically laminated rectangular plates with intermediate line supports", *Comput. Struct.*, **79**, 33-41.
Huang, S.C. and Hsu, B.S. (1993), "Modal analysis of a spinning cylindrical shell with interior point or circular line supports", *J. Vib. Acoust.*, **115**, 535-543.
Lee, H.P. and Ng, T.Y. (1995), "Dynamic stability of a plate on multiple line and point supports subject to pulsating conservative in-plane loads", *J. Sound. Vib.*, **185**, 345-356.
Li, Q.S. (2003), "An exact approach for free vibration analysis of rectangular plates with line-concentrated mass and elastic line-support", *In.t J. Mech. Sci.*, **45**, 669-685.
Li, S.R., Fu, X.H. and Batra, R.C. (2010), "Free vibration of three-layer circular cylindrical shells with functionally graded middle layer", *Mech. Res. Comm.*, **37**, 577-580.
Liew, K. M., Kitipornchai S. and Xiang, Y. (1995), "Vibration of annular sector Mindlin plates with internal radial line and circumferential arc supports", *J. Sound. Vib.*, **183**, 401-419.
Loy, C.T., Lam, K. Y. and Reddy, J. N. (1999), "Vibration of functionally graded cylindrical shells", *Int. J. Mech. Sci.*, 41, 309-324.
Matsunaga, H. (2009), "Free vibration and stability of functionally graded circular cylindrical shells according to a 2D higher-order deformation theory", *Compos. Struct.*, **88**, 519-531.
Miyamoto, Y., Kaysser, W.A., Brain, B.H., Kawasaki, A. and Ford, R.G. (1999), *Functionally graded materials: design, processing, and applications*, Kluwer Academic Publishers, Dordrecht, Netherlands.
Müller, E., Drašar, Č., Schilz, J. and Kaysser, W.A. (2003), "Functionally graded materials for sensor and energy applications", *Mater. Sci. Eng.*, **362**, 17-39.
Na, K.S. and Kim J.H. (2009), "Optimization of volume fractions for functionally graded panels considering stress and critical temperature", *Compos. Struct.*, **89**, 509-516.
Kadoli, R., Akhtar, K., and Ganesan, N. (2008), "Static analysis of functionally graded beams using higher order shear deformation theory", *Appl. Math. Model.*, **32**, 2509-2525.
Koizumi, M. (1997), "FGM activities in Japan", *Compos. B. Eng.*, **28**, 1-4.
Kokini, K., DeJonge, J., Rangaraj, S. and Beardsley, B. (2002), "Thermal shock of functionally graded thermal barrier coatings with similar thermal resistance", *Surf. Coating. Tech.*, **154**, 223-231.
Kong, J. and Cheung, Y.K. (1995), "Vibration of shear-deformable plates with intermediate line supports: a finite layer approach", *J. Sound. Vib.*, **184**, 639-649.
Pompe, W., Worch, H., Epple, M., Friess, W., Gelinsky, M., Greil, P., Hempel, U., Scharnweber, D. and Schulte, K. (2003), "Functionally graded materials for biomedical applications", *Mater. Sci. Eng.*, **362**, 40-60.
Pradhan, S.C., Loy, C.T., Lam, K.Y. and Reddy, J.N. (2000), "Vibration characteristics of functionally graded cylindrical shells under various boundary conditions", *Appl. Acoust.*, **61**, 111-129.
Qian, X.P. and Dutta, D. (2003), "Design of heterogeneous turbine blade", *Comput. Aided. Des.*, **35**, 319-329.
Soldatos, K.P. and Timarci, T. (1993), "A unified formulation of laminated composite, shear deformable, five-degrees-of-freedom cylindrical shell theories", *Compos. Struct.*, **25**, 165-171.
Soldatos, K.P. and Watson, P. (1997), "A method for improving the stress analysis performance of one- and two-dimensional theories for laminated composites", *Acta. Mech.*, **123**, 163-186.
Vel, S.S. (2010), "Exact elasticity solution for the vibration of functionally graded anisotropic cylindrical shells", *Compos. Struct.*, **92**, 2712-2727.

Veletsos, A.S. and Newmark, N.M. (1956), "Determination of natural frequencies of continuous plates hinged along two opposite edges", *J. Appl. Mech.*, **23**, 97-102.
Watari, F., Yokoyama, A., Omori, M., Hirai, T., Kondo, H., Uo, M. and Kawasaki, T. (2004), "Biocompatibility of materials and development to functionally graded implant for bio-medical application", *Compos. Sci. Tech.*, **64**, 893-908.
Woodward, B. and Kashtalyan, M. (2011), "Three-dimensional elasticity solution for bending of transversely isotropic functionally graded plates", *Eur. J. Mech. Solid.*, **30**, 705-718.
Wu, L.H., Jiang, Z.Q. and Liu, J. (2005), "Thermoelastic stability of functionally graded cylindrical shells", *Compos. Struct.*, **70**, 60-68.
Xiang, Y., Zhao, Y.B. and Wei, G.W. (2002a), "Exact solutions for vibration of multi-span rectangular Mindlin plates", *J. Vib. Acoust.*, **124**, 545-551.
Xiang, Y., Zhao, Y.B. and Wei, G.W. (2002b), "Levy solutions for vibration of multi-span rectangular plates", *In.t J. Mech. Sci.*, **44**, 1195-1218.
Zhao, X., Lee, Y.Y. and Liew, K.M. (2009), "Thermoelastic and vibration analysis of functionally graded cylindrical shells", *Int. J. Mech. Sci.*, **51**, 694-707.
Zhou, D. (1994), "Eigenfrequencies of line supported rectangular plates". *Int. J. Solid. Struct.*, **31**, 347-358.